To appear in ApJ Letters, April 10, 2000
Preprint typeset using LaTeX style emulateapj v. 04/03/99

HOT STARS AND COOL CLOUDS: THE PHOTODISSOCIATION REGION M16[1]

N. A. Levenson[2], James R. Graham[3], Ian S. McLean[4], E. E. Becklin[4], Donald F. Figer[5], Andrea M. Gilbert[3], James E. Larkin[4], Harry I. Teplitz[6,7], Mavourneen K. Wilcox[4]

To appear in ApJ Letters, April 10, 2000

ABSTRACT

We present high-resolution spectroscopy and images of a photodissociation region (PDR) in M16 obtained during commissioning of NIRSPEC on the Keck II telescope. PDRs play a significant role in regulating star formation, and M16 offers the opportunity to examine the physical processes of a PDR in detail. We simultaneously observe both the molecular and ionized phases of the PDR and resolve the spatial and kinematic differences between them. The most prominent regions of the PDR are viewed edge-on. Fluorescent emission from nearby stars is the primary excitation source, although collisions also preferentially populate the lowest vibrational levels of H_2. Variations in density-sensitive emission line ratios demonstrate that the molecular cloud is clumpy, with an average density $n = 3 \times 10^5\,\mathrm{cm}^{-3}$. We measure the kinetic temperature of the molecular region directly and find $T_{H_2} = 930$ K. The observed density, temperature, and UV flux imply a photoelectric heating efficiency of 4%. In the ionized region, $n_i = 5 \times 10^3\,\mathrm{cm}^{-3}$ and $T_{H\,II} = 9500$ K. In the brightest regions of the PDR, the recombination line widths include a non-thermal component, which we attribute to viewing geometry.

Subject headings: infrared: ISM: lines and bands — ISM: individual (M16) — molecular processes

1. INTRODUCTION

Star formation occurs in dense regions of the interstellar medium, and as a result, the environments of early-type stars often contain molecular clouds. In addition to creating an H II region, where hydrogen is predominantly ionized, stellar ultraviolet radiation creates a photodissociation region (PDR) when it interacts with molecular material. The feedback between extant stars and the nearby clouds in PDRs is important in regulating subsequent episodes of star formation. The UV flux determines the ionization fraction in molecular clouds, which in turn sets the ambipolar diffusion rate and thereby the rate of low-mass star formation (McKee 1989).

Hollenbach & Tielens (1997, 1999) comprehensively review the physical and chemical processes of PDRs. Far-ultraviolet (FUV) photons ($6 < h\nu < 13.6\,\mathrm{eV}$) dissociate molecules and excite the gas on the surface ($A_V < 3$) of the molecular cloud. The result is spatial stratification of molecular, atomic, and ionic components of a given element. At higher densities ($n \gtrsim 10^4\,\mathrm{cm}^{-3}$), collisional excitation also populates the excited states (Sternberg & Dalgarno 1989).

The columns of M16 (the Eagle Nebula) are PDRs. Most of the mass in the nebula is in molecular clouds, and a variety of molecular transitions are observed directly (Pound 1998; White et al. 1999). H_2 is observed on the cloud surfaces (Allen et al. 1999), and at the interface with the H II region, the columns are prominent in optical emission lines (Hester et al. 1996). The young cluster NGC 6611 contains many massive stars, which illuminate the columns with total FUV flux $16\,\mathrm{erg\,s^{-1}\,cm^{-2}}$ (Allen et al. 1999) from a distance of about 2 pc (Hester et al. 1996) .

We simultaneously observe the spatial and spectral relationship of the excited molecular and ionized phases of the PDR. Based on these observations (described in §2), we determine physical conditions in §3, and summarize the conclusions in §4.

2. OBSERVATIONS AND DATA REDUCTION

We obtained images and high resolution longslit spectra of the northernmost column of M16 using NIRSPEC, the facility near-infrared spectrometer on the Keck II 10-m telescope (McLean et al. 1998). Figure 1a identifies the observed region on the *Hubble Space Telescope* Hα image of M16 (Hester et al. 1996) with contours of integrated CO intensity (Pound 1998). We used the slit-viewing camera to image M16 on 1999 July 6 (UT), obtaining 9 exposures of 60 s each. In addition to the H_2 1-0S(1) filter, (bandpass 2.110–2.129 μm) the NIRSPEC-6 filter (1.558–2.315 μm) was in the optical path. We combined several observations of a blank field in the NIRSPEC-6 filter alone to use as a flat field and scaled this for sky subtraction from this crowded field. Figure 1b shows the resultant 2.12 μm image and the spectroscopy slit.

We employed the NIRSPEC-6 blocking filter and se-

[1] Data presented herein were obtained at the W.M. Keck Observatory, which is operated as a scientific partnership among the California Institute of Technology, the University of California and the National Aeronautics and Space Administration. The Observatory was made possible by the generous financial support of the W.M. Keck Foundation.

[2]Department of Physics and Astronomy, Johns Hopkins University, Baltimore, MD 21218

[3]Department of Astronomy, University of California, Berkeley, CA, 94720-3411

[4]Department of Physics and Astronomy, University of California, Los Angeles, CA, 90095-1562

[5]Space Telescope Science Institute, 3700 San Martin Dr., Baltimore, MD 21218

[6]Laboratory for Astronomy and Solar Physics, Code 681, Goddard Space Flight Center, Greenbelt MD 20771

[7]NOAO Research Associate

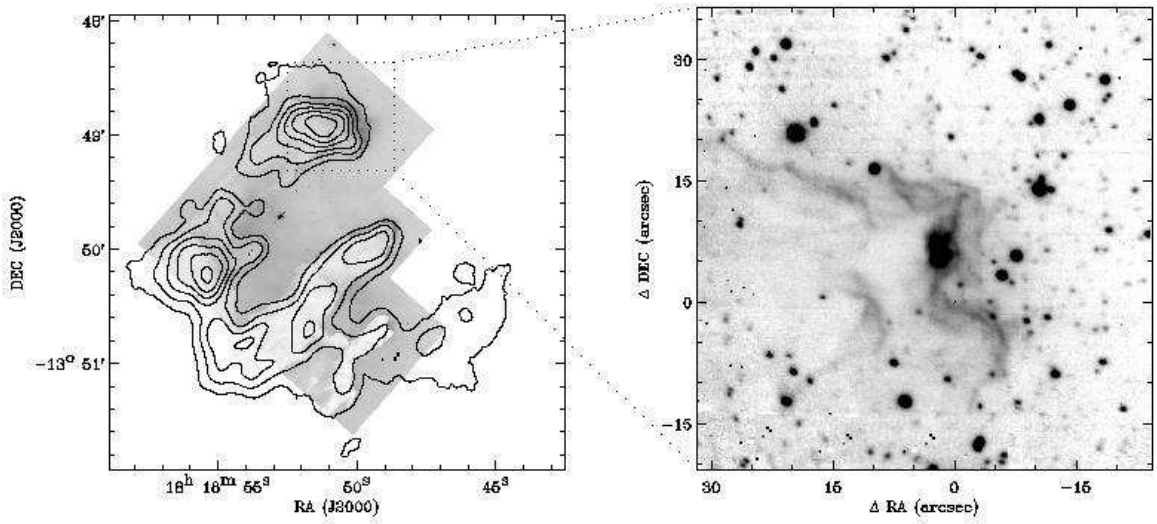

FIG. 1.— (a) The *HST* Hα image of M16 (Hester et al. 1996), with contours of integrated CO intensity (*solid lines*; Pound 1998) and the location of the NIRSPEC slit-viewing camera 2.12 μm image (*dotted line*) overlaid. The Hα image is scaled with a square-root stretch, and the CO contours are scaled linearly, from 50 to 300 Jy km s^{-1}. (b) Northern column of M16 at 2.12 μm (including H_2 1-0S(1)), observed with the NIRSPEC slit-viewing camera. Right ascension and declination are marked with respect to the observed center of the spectroscopy slit, which is overlaid. The UV flux comes from the northwest, which corresponds to the top of the slit in subsequent figures. The excited molecular emission is a surface phenomenon, arising only at the edge of the molecular cloud.

lected echelle and cross disperser positions to detect several H_2 rovibrational transitions, Brγ, and He I λ2.06 μm in our spectroscopic observations. We used the $0\farcs432 \times 24''$ slit at position angle 135° for resolution $\lambda/\Delta\lambda = 26,000$, where $\Delta\lambda$ is the observed $FWHM$ of an unresolved emission line. We obtained six exposures of 300 s each on the night of 1999 April 30 (UT), nodding along the slit between each exposure.

We subtracted a median dark frame from each image, divided by a flat field, and interpolated over deviant pixels, removing both cosmic rays and bad detector pixels. The spectra required rectification in both the spectral and spatial dimensions. We used the OH night sky lines and wavenumbers tabulated by Abrams et al. (1994) for wavelength calibration and the continuum emission of the telluric standard for spatial rectification. We observed HD 161056 and reduced the spectra similarly, then modelled this B1.5V star as a $T = 24,000$ K blackbody and interpolated over the stellar Brγ feature. We divided the M16 data by this spectrum to correct for atmospheric absorption and normalized the stellar spectrum from this $K = 5.4$ standard at 2.2 μm to flux calibrate the data.

Figure 2 contains the resultant two-dimensional spectra of several bright lines. We have subtracted off-source emission from each of these spectra. For the molecular emission, the background is near the edge of the slit toward the ionizing source, while for Brγ, the background lies away from the ionizing source. We list the complete set of detected lines, their vacuum wavelengths, their total fluxes in the slit, and their peak fluxes in Table 1.

3. PHYSICAL CONDITIONS

3.1. *Geometry*

The gross structure of the photodissociation region is evident in the images (Fig. 1) and two-dimensional spectra (Fig. 2). Fewer stars are observed directly through the cloud than in the surrounding region (Fig. 1b), implying $A_K > 1$. From the center of the molecular cloud out to the photoionizing source, distinct regions of quiescent molecular, excited molecular, atomic, and ionized material appear. The FUV photons do not fully penetrate the molecular cloud, so the excited H_2 resides only on the cloud's surface. The optically-thin ionized emission is brightest in the regions of highest density, near the cloud, and it is spatially more extended than the H_2 emission. The slit is aligned toward the ionizing source and covers several edges on the irregular surface of the cloud. Thus, we observe several distinct regions of photoevaporative flow. The greatest intensities are detected in the regions that are viewed edge-on.

In these observations, each of the bright regions within the PDR consists of spatially segregated molecular and recombination line emission. The two brightest regions at slit positions $-1\farcs2$ and $-3\farcs2$ in the 1-0S(1) emission, for example, are physically associated with the ionized emission at $7\farcs1$ and $3\farcs6$, respectively (Fig. 2d). (Note, however, that the more spatially extended Brγ peak at the top of slit includes some contribution from a nearby surface north of the slit, which we do not observe in H_2.) Moderate emission peaks appear at $2\farcs8$ and $1\farcs8$, and fainter surfaces at $-9\farcs3$, $-7\farcs9$, and $5\farcs3$ in the 1-0S(1) line. The first two of these are blended in the spatially extended Brγ emission, while the latter correspond to local emission maxima at $-2\farcs8$, $-0\farcs2$, and $11\farcs3$, so the projected separations of the H_2 and Brγ emission regions in the plane of the sky range from 1.8 to 2.5×10^{17} cm at the 2000 pc distance of M16 (Humphreys 1978; Hillenbrand et al. 1993). The transition from the atomic to molecular zone typically occurs at $A_V \sim 2$ (Tielens & Hollenbach 1985), or in terms of column density, $N_H \sim 4 \times 10^{21}$ cm^{-2}. Thus, the average gas density in the bright regions of the PDR is $1.6\text{–}2.2 \times 10^4$ cm^{-3}.

We determine the density in the ionized region and use the molecular line width (discussed below) to calculate the average density in the molecular region of the PDR.

Bertoldi & Draine (1996) show $n_i = S_{Ly}/(4\pi R^2 q c_i)$, where S_{Ly} is the Lyman continuum flux, R is the distance to the ionizing source, q accounts for attenuation of the ionization in the evaporative flow, and c_i is the isothermal sound speed in the ionized medium. We determine the value of $q \simeq 4.0 \times 10^{-14}\sqrt{S_{Ly} r}/R$ (Bertoldi 1989), where r is the cloud radius. We find the density of the ionized region $n_i = 5.2 \times 10^3\,\mathrm{cm}^{-3}$, for $c_i = 12\,\mathrm{km\,s}^{-1}$ (calculated for $T_{H\,II} = 9500$ K, below) and $r = 25''$. For pressure balance across the ionization front, $n \simeq 2 n_i c_i^2/(\Delta v/2.35)^2$, where Δv is the $FWHM$ of the molecular line width, so in the molecular region, $n \simeq 3.2 \times 10^5\,\mathrm{cm}^{-3}$. This is significantly greater than the density calculated above, which integrated over contributions from the ionized to the molecular region. Here, n is determined in the molecular zone alone, which should be denser.

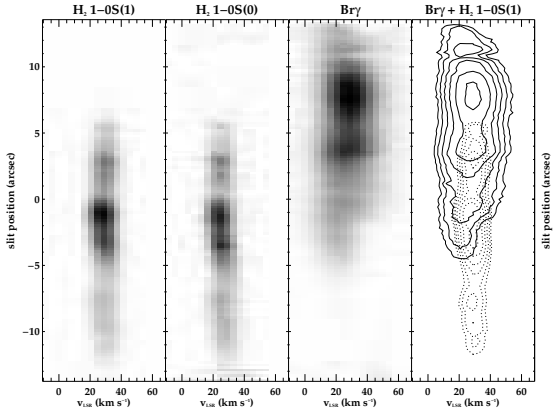

FIG. 2.— Two-dimensional spectra of bright lines. (a) H_2 1-0S(1), 2.12 μm, scaled linearly from 0 to 5.0×10^{-15} erg s^{-1} cm^{-2} arcsec^{-2}. (b)H_2 1-0S(0), 2.22 μm, scaled linearly from 0 to 1.8×10^{-15} erg s^{-1} cm^{-2} arcsec^{-2}. (c) Brγ, 2.17 μm, scaled linearly from 0 to 3.6×10^{-15} erg s^{-1} cm^{-2} arcsec^{-2}. (d) Contours of Brγ (*solid lines*) and H_2 1-0S(1) (*dotted lines*) emission, in logarithmic intervals from 0.6 to 3.4×10^{-15} erg s^{-1} cm^{-2} arcsec^{-2}. The Brγ emission is broader and closer to the ionizing source (located at the top of the slit) than the molecular lines. The two brightest regions in Brγ at slit positions 3.″6 and 7.″1 correspond to the H_2 peaks at $-3.''2$ and $-1.''2$, respectively.

3.2. *Kinematics*

The various gas phases exhibit distinct kinematic structure. We measure the line profiles at slit position 3.″2 in 1-0S(1) emission, which is clearly distinguished in the Brγ and He emission at 3.″6. Because we observe this PDR nearly edge-on, the central velocities of the H_2^* and ionized material are not significantly different; the average motion occurs in the plane of the sky. We measure $v_{LSR} = 29\,\mathrm{km\,s}^{-1}$ for this 1-0S(1) feature and $v_{LSR} = 28\,\mathrm{km\,s}^{-1}$ in Brγ. In H_2, $\Delta v = 4.6 \pm 0.1\,\mathrm{km\,s}^{-1}$, $\Delta v = 29.0 \pm 0.2\,\mathrm{km\,s}^{-1}$ in Brγ, and $\Delta v = 18.7 \pm 0.2\,\mathrm{km\,s}^{-1}$ in He I $\lambda 2.06\mu$m, after correcting for the instrumental profile. In the molecular gas, the velocity width corresponds to a kinetic temperature $T_{H_2} = 930 \pm 50$ K. This value is reasonable near the edge of the cloud in the H_2^* zone where maximum temperature of the PDR occurs (Tielens & Hollenbach 1985).

Accounting for the mass difference between H and He demonstrates that these line widths are not purely thermal, however. Assuming that they each consist of a macroscopic component that is independent of molecular weight in addition to the thermal component, we find $\Delta v_{macro} = 12.2\,\mathrm{km\,s}^{-1}$. For Br$\gamma$, $\Delta v_{therm} = 25.6\,\mathrm{km\,s}^{-1}$, and $T_{H\,II} = 14000 \pm 230$ K. This temperature is hotter than typically observed in H II regions, but several factors tend to increase $T_{H\,II}$ at the PDR-H II interface: increased photoelectric heating near a greater population of grains; the harder radiation field, which reduces the contribution of significant low-ionization coolants, such as O^+; and increased density, which reduces the radiative cooling rate by increasing the collisional de-excitation rate (e.g., Spitzer 1978).

The non-thermal recombination line widths may also be attributable to bulk motion of material flowing off the cloud surface. In the bright region discussed above, we view the PDR nearly edge-on, along a line of sight that includes both redshifted and blueshifted velocity components of the material that evaporates off the curved surface of the cloud. When the view of the PDR is closer to face-on, the intensity is less enhanced, and only the blueshifted velocity component arises. This is the case for the minor emission peaks at the bottom of the slit, which occur on the near surface of the cloud. These central velocities are slightly lower (by approximately $7\,\mathrm{km\,s}^{-1}$) than those of the brightest peaks, and the observed widths are narrower. At slit position $-2.''8$, for example, we find $\Delta v = 20.9 \pm 0.2$ and $10.1 \pm 0.2\,\mathrm{km\,s}^{-1}$ in Brγ and He I, respectively. These both correspond to kinetic temperature $T_{H\,II} = 9500 \pm 180$ K. If this is a more accurate measurement of the temperature at the edge of the H II region, then we have underestimated the contribution of the non-thermal velocity component above. While $T_{H\,II}$ at the interface is likely higher than the typical temperatures in the diffuse central portions of H II regions, as argued above, it may be less than 14,000 K.

3.3. *H_2 Excitation*

In a PDR, UV pumping is the primary source of H_2 excitation. In M16, such fluorescent emission obviously occurs. A variety of lines that originate in high vibrational levels v are observed, including 7-5O(4) and 3-2S(5) (Table 1), whereas thermal population of these high-v levels would dissociate the molecules. We detect emission from all of the strong transitions in our bandpass that Black and van Dishoeck (1987) predict, except those originating in levels $v \geq 9$ or lie in regions of poor atmospheric transparency.

Collisional excitation is also important, however. The ratio of line intensities I(1-0S(1))/I(2-1S(1))= 2–5, and the average ratio over the slit is 4. As we found above in §3.1, this requires $n > 10^4\,\mathrm{cm}^{-3}$ (Burton, Hollenbach, & Tielens 1990), so collisions aid in populating the $v = 1$ level. We do not, however, observe line ratios as high as Allen et al. (1999), who find I(1-0S(1))/I(2-1S(1))> 10 in similar regions with Fabry-Perot imaging. We expect our results to be more accurate, having better flux calibration and simultaneous sky measurements.

Line ratios also directly measure excitation temperatures. Across the slit, we find from the 1-0S(1) and 2-1S(1) lines vibrational temperature $T_{vib} = 3000$–3800 K, with a median $T_{vib} = 3400$ K. Using I(1-0S(1))/I(1-0S(3)), we find rotational temperature $T_{rot} = 1600$–2100 K and median $T_{rot} = 1800$ K. Comparing I(1-0S(1))/I(1-0S(0)), $T_{rot} = 450$–870 K, with a median $T_{rot} = 580$ K. The relatively low value of T_{vib} and relatively high value of T_{rot} (particularly in the brightest regions) distinguish the M16 PDR from purely fluorescent emission in a low den-

sity medium, where $T_{vib} \sim 5500$ and $T_{rot} \sim 1400$ from I(1-0S(1))/I(1-0S(3)) are typical.

We compare the line intensities of the three brightest regions with the models of Draine & Bertoldi (1996). Considering all observed lines, all three regions are best fit with $\chi/n = 0.1\,\mathrm{cm}^3$, and $T_0 = 1000$ K, where χ measures the incident UV flux ($\chi = 1$ is the Habing [1968] flux), and T_0 is the temperature at the edge of the PDR. The observed line ratios clearly rule out models of a weak field ($\chi \leq 10^3$) and low density ($n \leq 10^4\,\mathrm{cm}^{-3}$). Both $\chi = 10^4$ and $\chi = 10^5$ are acceptable. For consistency with other density measurements and the UV field expected from members of NGC 6611, $\chi = 10^4$ and $n = 10^5\,\mathrm{cm}^{-3}$ is the preferred model. Although the grid of models is coarse, we identify trends by contrasting these regions. For example, the variation of density-sensitive line ratios along the spatial extent of the slit demonstrates that the cloud density is not constant. The decreased ratios I(1-0S(1))/I(1-0S(0)) and I(1-0S(1))/I(2-1S(1)) at slit position $-3\farcs2$ relative to slit position $-1\farcs2$ show that the former region has lower density.

In thermal equilibrium, the ratio of ortho-hydrogen (having odd rotational level, J) to para-H_2 (having even J) is 3, and only collisions can change the ortho:para ratio. This abundance ratio is therefore a significant parameter in PDRs and affects the emission line ratios. We calculate the ratio of ortho-H_2 and para-H_2 from the 1-0S(1) and 1-0S(0) lines, finding ratios of 1.3–2.2, with an median value of 1.7. Because UV pumping of the damping wings of optically thick lines populate the excited levels, the expected ratio of column densities in the vibrationally excited levels is 1.7, while the true ortho:para abundance is 3 (Sternberg & Neufeld 1999).

The photoelectric effect on interstellar grains is likely to be the primary heating source in PDRs, but its exact process is uncertain. We determine the efficiency of converting FUV flux to photoelectric heating, ϵ, assuming thermal equilibrium. Emission in the [O I] 63 μm and [C II] 158 μm fine structure lines cools the gas. For the measured temperature and density, we calculate a net cooling rate $\Lambda = 4.2\times10^{-17}\,\mathrm{erg\,s^{-1}\,cm^{-3}}$ in M16, with 96% due to [O I]. In the parameterization of Bakes & Tielens (1994), the heating function $\Gamma = 10^{-24} n\epsilon\chi\,\mathrm{erg\,s^{-1}\,cm^{-3}}$. Thus, we find $\epsilon = 0.042$, for $\chi = 9700$ (Allen et al. 1999). The theoretical prediction, $\epsilon = 0.016$ (Bakes & Tielens 1994), is a function of $\chi\sqrt{T}/n_e$, where n_e is the electron density. We have assumed that the ionization of carbon provides the electrons; increasing n_e would increase ϵ, without significantly altering the cooling rate. Alternatively, decreasing the gas to dust ratio would allow a lower efficiency in equilibrium with the cooling rate we predict.

4. CONCLUSIONS

Spectroscopy of M16 with NIRSPEC offers the advantage of simultaneous observation of both the molecular and ionized phases of its photodissociation regions. At high resolution, we detect the spatial and kinematic signatures of photoexcitation of molecular material. Most of the emission is due to distinct regions of photodissociation on the molecular cloud's surface that we observe edge-on. The spectrum includes several lines that originate in high vibrational levels, which demonstrates that fluorescent excitation predominates. The density $n \sim 10^5\,\mathrm{cm}^{-3}$ and varies among the emitting regions, so collisions also preferentially populate low-lying vibrational levels. We measure kinetic temperature $T_{H_2} = 930$ K in the molecular gas, which requires efficient photoelectric heating near the cloud's surface. In the spatially-segregated ionized region, $T_{H\,II} = 9500$ K, and the velocity widths of the brightest regions include a macroscopic contribution.

It is a pleasure to acknowledge the hard work of past and present members of the NIRSPEC instrument team at UCLA: Maryanne Angliongto, Oddvar Bendiksen, George Brims, Leah Buchholz, John Canfield, Kim Chin, Jonah Hare, Fred Lacayanga, Samuel B. Larson, Tim Liu, Nick Magnone, Gunnar Skulason, Michael Spencer, Jason Weiss, and Woon Wong. In addition, we thank the Keck Director Fred Chaffee, CARA instrument specialist Thomas A. Bida, and all the CARA staff involved in the commissioning and integration of NIRSPEC. We especially thank our Observing Assistants Joel Aycock, Gary Puniwai, Charles Sorenson, Ron Quick, and Wayne Wack for their support. We thank Amiel Sternberg for helpful discussions and Marc Pound for providing his CO data.

REFERENCES

Abrams, M. C., Davis, S. P., Rao, M. L. P., Engleman, R., Jr., & Brault, J. W. 1994, ApJS, 93, 351
Allen, L. E., Burton, M. G., Ryder, S. D., Ashley, M. C. B., & Storey, J. W. V. 1999, MNRAS, 304, 98
Bakes, E. L. O., & Tielens, A. G. G. M. 1994, ApJ, 427, 822
Bertoldi, F. 1989, ApJ, 346, 735
Bertoldi, F., & Draine, B. T. 1996, ApJ, 458, 222
Black, J. H., & van Dishoeck, E. F. 1987, ApJ, 322, 412
Burton, M. G., Hollenbach, D. J., & Tielens, A. G. G. M. 1990, ApJ, 365, 620
Draine, B. T., & Bertoldi, F. 1996, ApJ, 468, 269
Habing, H. J. 1968, Bull. Astron. Inst. Netherlands, 19, 421
Hester, J. J., et al. 1996, AJ, 111, 2349
Hillenbrand, L. A., Massey, P. Strom, S. E., & Merrill, K. M. 1993, AJ, 106, 1906
Hollenbach, D. J., & Tielens, A. G. G. M. 1997, ARA&A, 35, 179
Hollenbach, D. J., & Tielens, A. G. G. M. 1999, Rev. Mod. Phys. 71, 173
Humphreys, R. M. 1978, ApJS, 38, 309
McKee, C. F. 1989, ApJ, 345, 782
McLean, I. S., et al. 1998, Proc. SPIE, 3354, 566
Pound, M. W. 1998, ApJ, 493, L113
Spitzer, L., Jr., 1978, *Physical Processes in the Interstellar Medium*, (New York: Wiley)
Sternberg, A., & Dalgarno, A. 1989, ApJ, 338, 197
Sternberg, A., & Neufeld, D. A. 1999, ApJ, 516, 371
Tielens, A. G. G. M., & Hollenbach, D. 1985, ApJ, 291, 722 (TH)
White, G. J., et al. 1999, A&A, 342, 233

TABLE 1
OBSERVED LINES

Transition	Wavelength [μm]	Total Flux [erg s^{-1}cm^{-2}]	Peak Surface Brightness [erg s^{-1}cm^{-2}arcsec^{-2}]
H_2			
7-5O(4)	1.94343	$3.9 \pm 0.2 \times 10^{-16}$	$1.9 \pm 0.4 \times 10^{-16}$
2-1S(5)	1.94486	$1.1 \pm 0.01 \times 10^{-14}$	$3.2 \pm 0.2 \times 10^{-15}$
1-0S(3)[a]	1.95756	$5.6 \pm 0.02 \times 10^{-14}$	$4.8 \pm 0.2 \times 10^{-15}$
3-2S(5)	2.06556	$4.5 \pm 0.06 \times 10^{-15}$	$3.7 \pm 0.6 \times 10^{-16}$
8-6O(4)	2.12155	$7.4 \pm 0.2 \times 10^{-16}$	$1.2 \pm 0.3 \times 10^{-16}$
1-0S(1)	2.12183	$6.2 \pm 0.02 \times 10^{-14}$	$5.3 \pm 0.2 \times 10^{-15}$
3-2S(4)	2.12799	$1.9 \pm 0.04 \times 10^{-15}$	$2.4 \pm 0.5 \times 10^{-16}$
1-0S(0)	2.22329	$2.4 \pm 0.01 \times 10^{-14}$	$1.6 \pm 0.1 \times 10^{-15}$
2-1S(1)	2.24772	$1.6 \pm 0.01 \times 10^{-14}$	$1.3 \pm 0.1 \times 10^{-15}$
Recombination Lines			
Brγ	2.16609	$1.3 \pm 0.003 \times 10^{-13}$	$3.7 \pm 0.2 \times 10^{-15}$
Brδ[a,b]	1.94509	$2.3^{+1}_{-0.02} \times 10^{-14}$	$1.3 \pm 0.1 \times 10^{-15}$
He I	2.05869	$9.7 \pm 0.03 \times 10^{-14}$	$3.9 \pm 0.2 \times 10^{-15}$
He I	2.11259	$2.6 \pm 0.05 \times 10^{-15}$	$1.9 \pm 0.4 \times 10^{-16}$

[a]Correction for atmospheric transparency is large, around 2

[b]Missing flux due to poor atmospheric transparency